Acceleration of vortex-particle simulations using a pseudo-particle method

Acceleration of vortex-particle simulations using a pseudo-particle method

F Thönnißen[1], E K Fritz[1,2], W Schröder[1]

[1] Chair of Fluid Mechanics and Institute of Aerodynamics, RWTH Aachen University, Wüllnerstraße 5a, 52062 Aachen (Germany)
[2] TNO Energy Transition, Westerduinweg 3, 1755 LE Petten (The Netherlands)

E-mail: f.thoennissen@aia.rwth-aachen.de

Abstract. Vortex methods like vortex-lattice or vortex-panel methods are particularly promising to enhance the industrial aerodynamic design process of modern wind turbines. However, despite their advantages over low order methods, like the blade-element-momentum theory, vortex methods share an essential disadvantage. Their computational cost rapidly increases, which is due to their n-body problem characteristics. To overcome this issue, a method that neither relies on multipole expansions nor on a multi-grid approach is presented. Based on the aerodynamic simulation of the MEXICO rotor, it is shown that the proposed vortex pseudo-particle method (VPPM) is able to reduce the computational cost related to the n-body problem of vortex methods to $\mathcal{O}(n \times log(n))$. However, its application is not only advantageous in terms of the reduction of the computational cost. Since vortex- and pseudo-particles share the same properties, the VPPM's implementation is quite simple compared to that of fast multipole methods. Furthermore, no method specific boundary-conditions need to be imposed as in the case of multi-grid methods. Therefore, the presented pseudo-particle approach is an attractive alternative to fast multipole or multi-grid methods.

1. Introduction

The iterative character of the industrial design process of modern wind turbines requires efficient and economic tools to optimally harmonize wind turbine components. Therefore, the aeroelastic load calculation in the industrial sector almost entirely relies on blade-element-momentum theory (BEMT) based approaches. Apart from their low computational cost, several decades of experience have strengthened confidence in these methods. However, while their level of uncertainty is low for normal design conditions, experiments [1] showed that the uncertainty is higher for off-design conditions, e.g., at yawed inflow. In these off-design cases, the uncertainty often depends on the validity range and the interconnection of submodels which are used to describe the influence of flow phenomena that are not inherently captured by the BEMT. Although higher-order methods like Reynolds-averaged Navier-Stokes (RANS) solvers or large-eddy simulations (LES) can be used to cover these issues in research institutions, they are often not applicable in industry since the computing resources are high for RANS and extraordinarily high for LES solutions. In conclusion, there is a demand for medium-order methods representing a compromise between computing time and accuracy. Vortex methods like vortex-lattice or vortex-panel methods are particularly promising to close this gap. Unlike BEMT-based approaches, the number of required submodels is significantly lower for these methods, which reduces the level of

uncertainty. While vortex-lattice models solely describe the turbine's wake evolution in time, vortex-panel methods additionally provide the blade's surface pressure distribution. If the influence of viscous effects on the pressure distribution is captured by means of a boundary layer model, panel methods represent a viable tool for the iterative aerodynamic optimization of a wind turbine's rotor blades [2]. Furthermore, the pressure distribution can be used as an input for a medium-order (e.g. a shear panel approach) or a higher-order structural solver (e.g. a finite-element solver) to capture the blade's aeroelastic behavior.
However, despite their advantages over BEMT based approaches, vortex-lattice and vortex-panel methods have an essential disadvantage that is linked to the vortex rings, which are used to capture the evolution of the turbine's wake in time. Their computational cost rapidly increases with each simulation time step since they are proportional to the squared number of vortex rings, which defines an n-body problem. Using an equivalent vortex-particle representation of the vortex rings allows to apply a fast multipole method (FMM) or a multi-grid based approach. The FMM makes use of multipole expansions to approximate the vortex particles' influence [3], [4] while it is interpolated on a set of increasing coarser spatial meshes in case of a multi-grid method (MGM) [5], [6], [7]. Both methods exploit octree structures to hierarchically subdivide the computational domain and to theoretically reduce the computational cost from $\mathcal{O}(n^2_{Particles})$ to $\mathcal{O}(n_{Particles})$.
In this article, another promising method, which also leads to a significant reduction of the computational cost is presented. The simplicity of the approach makes it an attractive alternative to FMM or MGM. It is based on the work of Anderson [8] and Makino [9]. Unlike FMM or MGM, it neither relies on multipole expansions nor on the multi-grid approach.

2. Methodology

The following section outlines the numerical setup of the presented approach, which makes use of a coupled vortex-panel/vortex-particle method. Furthermore, the concept of pseudo-particles is introduced in detail. The configuration of all models is given in Tab. 1. All routines were implemented in MathWorks MATLAB. The graphical processing unit (GPU) of a GeForce RTX 2080 TI graphics card was used to evaluate the induced velocity of the vortex and pseudo particles (Eq. 4). These calculations were performed in single precision. All other operations were processed in double precision by one core of an Intel I7 9700 processor.

2.1. Vortex-panel method

To determine the flow field in the vicinity of the rotor blades, a vortex-panel method is applied. A rotor blade's surface is represented using quadrilateral surface elements referred to as panels. Each panel holds a set of singular elements (constant vortex ring/constant source) which are solutions to Laplace's equation. By imposing the kinematic boundary condition on the body's surface and the Kutta condition at the blade's trailing edge, the strength of these elements is determined. During this step a new row of panels referred to as wake panels is shed at the blade's trailing edge, where each wake panel holds a vortex ring. These wake panels move in space according to the local velocity of the flow field, which equals the sum of the freestream velocity, the blade's induced velocity, and the velocity induced by all wake panels that were shed in the previous time steps. For a more detailed discussion of the implemented vortex-panel method the reader is referred to Katz et al. (s. Ch. 13.13) [10].

2.2. Vortex-particle method

By taking the curl of the Navier-Stokes equation for incompressible unsteady flows the vorticity transport equation is obtained, which describes the evolution of a fluid's vorticity field. Vortex-particle methods are used to trace this evolution in a Lagrangian framework by representing the

vorticity field by a set of particles. Each particle accounts for a fraction of the vorticity field $\vec{\omega}$, while its strength $\vec{\alpha}_p$ equals the integral of the vorticity $\vec{\omega}$ over a small material volume V_p of the field:

$$\vec{\alpha}_p = \int_{V_p} \vec{\omega}(t)\,\mathrm{d}V = \Gamma \mathrm{d}\vec{l}. \tag{1}$$

The particles evolution in time is governed by

$$\frac{d\vec{x}_p}{dt} = \vec{u}_p(\vec{x}_p, t) \tag{2}$$

$$\frac{d\vec{\alpha}_p}{dt} = (\vec{\alpha}_p(t) \cdot \nabla^T)\vec{u}_p(\vec{x}_p(t), t). \tag{3}$$

Eq. 3 is referred to as the transpose scheme. Note that other schemes do exist [11]. The induced velocity is obtained by

$$\vec{u}_p(\vec{x}, t) = -\sum_p \frac{q(\rho)}{|(\vec{x} - \vec{x}_p(t))|^3}(\vec{x} - \vec{x}_p(t)) \times \vec{\alpha}_p(t), \tag{4}$$

where $q(\rho) = q(|\vec{x} - \vec{x}_p(t)|/\sigma)$ is a 3D regularization function with σ being a cut-off radius. Within the scope of this work the high order algebraic kernel proposed by Winkelmans et al. [11] is used. For a more detailed discussion of vortex-particle methods the reader is referred to [11], [12], [13].

In the presented approach, the wake panels of the vortex-panel method are converted into an equivalent vortex-particle representation five time steps after their creation, see Fig. 1. During this process the wake panel's edges are divided into segments of equal lengths Δl and a particle is positioned at the center of each segment. Let Γ be the circulation of the wake panel to be converted, the particles strength α is calculated using Eq. 1. To ensure the communication between the particles and maintaining the integrity of the Lagragian approach, a certain overlap of the particles is needed. Therefore, the particles core radius is set to $\sigma = \kappa\Delta l$, where $\kappa = 1.5$.

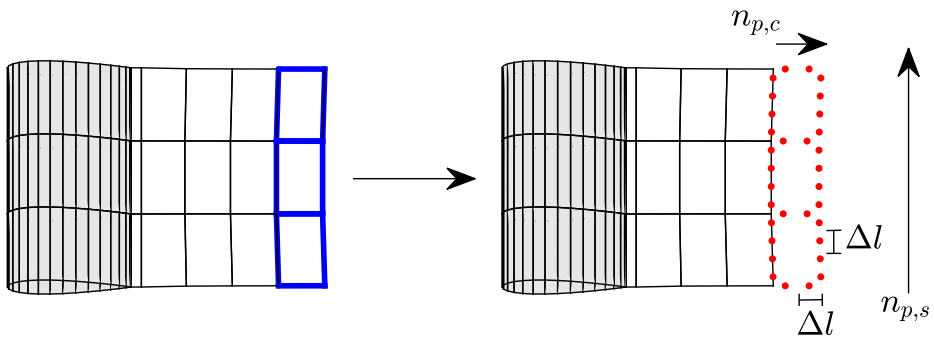

Figure 1: Wake panels of the vortex-panel method (blue) are converted into an equal vortex-particle representation (red), five time steps after their creation.

Since the particle-based representation of the vorticity field is not guaranteed to be solenoidal as time evolves, the filtering method proposed by Pedrizetti [14] is used to tackle this problem.

Let ω be the divergence-free vorticity field, which can be reconstructed from the velocity field and a relaxation factor τ, the particle strength evolves as

$$\vec{\alpha}_{p,t+1}(t) = (1-\tau)\vec{\alpha}_p(t) + \tau\frac{\vec{\omega}(\vec{x}_p(t),t)}{||\vec{\omega}(\vec{x}_p(t),t)||}||\vec{\alpha}_p(t)||. \tag{5}$$

2.3. Pseudo-particle method

Multiple methods have been developed to reduce the computational cost of n-body problems, e.g., the Barnes-Hut algorithm [15], the Fast Multipole Method (FMM), [3] and the Poisson Integral Method by Anderson [8]. The latter is used in the presented pseudo-particle method. All these methods rely on the fact that the influence of a vortex particle on its surroundings strongly decays with growing distance to the point of interest. If this distance is large compared to a characteristic length, e.g. the radius of a sphere enclosing a number of N particles, the particles' influence can be approximated through finite series expansions, represented by a much smaller number of M computational elements, e.g. one single multipole. Since $M \ll N$, the evaluation of M computational elements typically takes much less effort than that computing the influence of N particles. By approximating fractions of the $N \times N$ interactions, the computational cost are reduced significantly. This concept is also used by the pseudo-particle method since the influence of N particles inside a sphere is approximated by K pseudo-particles, which are located on the sphere's surface, where $K \ll N$.

Let (r_i, Θ_i, ϕ_i) be a vortex particle's polar coordinates with respect to the center of a sphere with radius r, γ_i the angle between a vortex- and a pseudo-particle, p the cut-off order, α_i the strength of a vortex particle i, α_j the strength of a pseudo-particle j, and P a Legendre polynomial. Then, the strength of N vortex particles in a cluster is interpolated to a number of K integration points (Eq. 6) on the clusters surrounding sphere (Fig. 2a). These points can be distributed freely on the sphere's surface. However an equidistant distribution of the integration points is favorable to capture the vortex particles' influence.

$$\alpha_j = \frac{1}{4\pi K}\sum_{k=0}^{p}\sum_{m=-k}^{k}\beta_k^m Y_k^{-m}(\theta_j,\phi_j), \tag{6}$$

$$\beta_k^m = \sum_{i=1}^{N}\alpha_i r_i^k Y_k^{-m}(\theta_i,\phi_i), \tag{7}$$

$$Y_k^m(\theta,\phi) = (-1)^m\sqrt{\frac{2k+1}{4\pi}\frac{(k-|m|)!}{(k+|m|)!}}\,P_k^m(\cos\theta)\,e^{im\phi}. \tag{8}$$

The information accumulated in an integration point is captured by a pseudo-particle, which shares the same properties as vortex particles. To avoid the triple summation over *i,k,m* the addition theorem of spherical harmonics is applied [9] and the pseudo-particles strength is expressed as

$$\alpha_j = \frac{1}{K}\sum_{i=1}^{N}\alpha_i\sum_{l=0}^{p}(\frac{r_i}{r})^l P_l(cos\gamma_i). \tag{9}$$

For the efficient application of the pseudo-particle method an octree structure is used to hierarchically subdivide the computational domain. In each time step of the simulation the domain of particles is subdivided using a length parameter l_{Top}, which defines the size of the boxes on the top level of the octree (s. Fig. 2b). If the number of particles n_P in a box

exceeds a predefined threshold of $n_{P,Box}$ particles, the box is divided into eight sub cells with the particles being distributed to the cells. This process is recursively repeated for each of the sub cells. Subsequently, an enclosing sphere is defined for each box on every level of the octree. Its radius equals half of the largest space diagonal of the box multiplied by a predefined factor m_r. This sphere is used in the subsequent mapping of the vortex particles' influence through pseudo-particles. At the end of this initial sweep of the octree, each box features a pseudo-particle representation of the vortex particles it encloses. Note that there is no translation of the pseudo-particles' influence like the translation operations used in FMMs.
To evaluate the influence of $N \times N$ vortex particles on each other, hereinafter referred to as P2P-interaction, the boxes on the lowest level of the octree are selected one by one as a target box. Afterwards, the octree is passed from top to bottom to calculate the overall particles' influence on the specific subset of particles inside the target box. During this step the boxes that are well-separated from the target box by the criterion

$$|\vec{x}_{center,target-box} - \vec{x}_{center,source-box,i}| < m_d \times r_{sphere,i} \tag{10}$$

are determined. The influence of the boxes satisfying this criterion can be evaluated using their corresponding set of pseudo-particles. These pseudo-particles and the vortex particles of the boxes that are not well-separated are added to one joint list, the interaction list. Once the octree has been swept, the interaction list particles' influence on the target particle set is evaluated. Since vortex- and pseudo-particles share the same properties, the influence of the interaction list particles can be evaluated using the same equation (Eq. 4). This constitutes a significant advantage since all particles and their properties can be stored in a unified global data structure. Therefore, only the indices of the particles need to be exchanged during the sweep, which reduces memory operations.

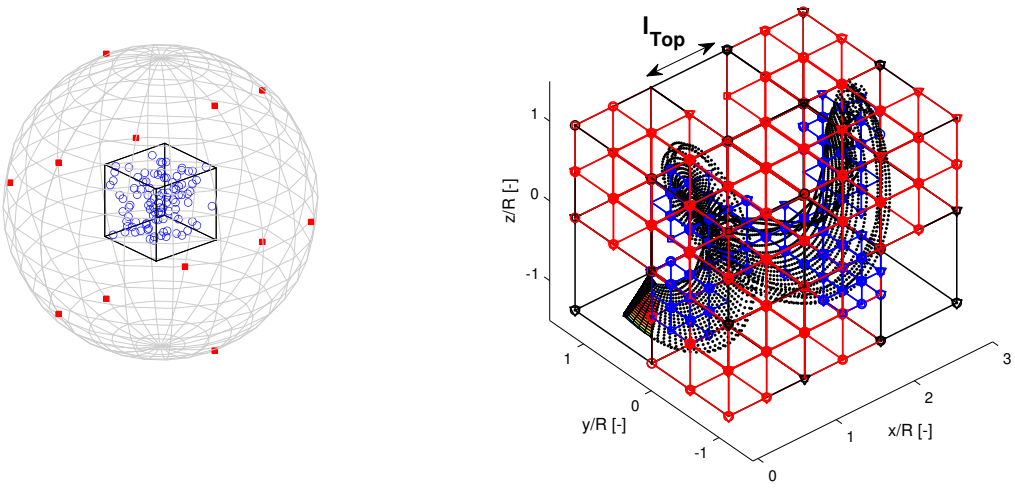

(a) (b)

Figure 2: Mapping of the vortex particles (blue) contained in a box as pseudo-particles (red) on the surface of an enclosing sphere (a) and exemplary illustration of the subdivision of the computational domain using an octree structure for the case of one single rotating blade (b)

General	Azimuthal step size	$\Delta\Theta$	6	$^\circ$
	Time step size	Δt	0.0024	s
	Number of revolutions	n_{Rounds}	25	-
	Turbine radius	R	2.25	m
	Rotational speed	ω_{rot}	44.45	rad/s
	Tip-speed ratio	λ	[4.16,6.66,9.99]	-
Flow properties	Free-stream velocity	v_∞	[24,15,10]	[m/s]
	Reynolds number	Re	∞	-
Vortex-panel method	Spanwise discretization	$n_{Sections}$	20	-
	Chordwise discretisation	n_{Panels}	60	-
Vortex-particle method	Wake Panel			
	segment length	Δ_l	0.038	m
	spanwise discretization	$n_{P,s}$	60	-
	chordwise discretization	$n_{P,c}$	10	-
	Core radius	σ	0.056	m
	Overlap factor	κ	1.5	-
	Relaxation factor	τ	0.05	-
Pseudo-particle method	Number of integration points / pseudo-particles per box	K	50	-
	Cut-off order	p	9	-
	Threshold factor	m_d	2	-
	Sphere radius multiplier	m_r	1.5	-
	Number of particles per box	$n_{P,Box}$	5000	-
	Top level box length	l_{Top}	2.25	-

Table 1: Configuration of the overall simulation and submodels

3. Results

The efficiency of the described vortex pseudo-particle method was evaluated by simulating the flow field of the MEXICO rotor [1] for several tip-speed ratios. For each tip-speed ratio, 25 rotor revolutions with an azimuthal step size of $\Delta\Theta = 6^\circ$ are simulated. The blade geometry is resolved by 20 sections in spanwise direction, where each section consists of 60 panels.

3.1. Performance of the VPPM

Figure 3a shows the needed wall time T to calculate the induced velocity due to the particle-on-particle interaction (P2P) as a function of the number of particles for several tip-speed ratios $\lambda = [4.16, 6.66, 9.99]$. Compared to the direct calculation of the vortex-particle method (VPM), the wall time required by the VPPM is lower for the number of particles $n_{P,BE} > [150000, 200000, 270000]$ for $\lambda = [4.16, 6.66, 9.99]$. The cumulative wall time ratio T_c

$$\widetilde{T_c} = \frac{\sum_i^n T_{i,VPPM}}{\sum_i^n T_{i,VPM}} \tag{11}$$

for the total simulation of 25 rotor revolutions is reduced by nearly [50%,36%,28%], see Fig. 3b. This reduction is due to the approximation of fractions of the P2P-interaction in case of the VPPM. Let $m_{P,VPPM,i}$ be the number of vortex- and pseudo-particles that interact with a number of $n_{P,VPPM,i}$ particles inside a target box i at the lowest level of the octree, the decrease in the number of P2P-interactions is quantified by the work load ratio $\widetilde{W}$

$$\widetilde{W} = \frac{\sum_i^{nBoxes} m_{P,VPPM,i} \times n_{P,VPPM,i}}{n_P^2}. \tag{12}$$

Its progress is depicted in Figure 3b. It appears that $\widetilde{W}$ rapidly drops below a value of $\widetilde{W} = 1$. However, the break-even point of the wall time ratio $\widetilde{T} = T_{VPPM}/T_{VPM} = 1$ is not reached at the same time. This is due the overhead that is caused by the setup of the octree, the particle mapping, and the sweep of the octree. Its computational effort is quantified by its wall time T_o, which strongly depends on the upper limit of particles per box $n_{P,Box}$ of the octree. The influence of the parameter $n_{P,Box}$ on the wall time T, the overhead time T_o, and the work load ratio $\widetilde{W}$ is depicted in Figure 4a. Based on the reference case of $n_{P,Box,ref} = 5000$ a decrease of $n_{P,Box}$ results in a decrease of $\widetilde{W}$ due to the octrees refinement, which is linked to a reduction of $n_{P,Box}$. Each box that exceeds a predefined threshold of $n_P > n_{P,Box}$ particles is divided into eight sub cells. In case of $n_{P,Box} = 1000$ the octree structure is refined five times during the simulation, which is observed as five sudden steps in the trend of $\widetilde{W}$ and T_o. Since the boxes become smaller during each refinement the number of boxes that meet the distance criterion Eq. 10 rises. Consequently, the number of P2P-interactions is reduced since the influence of an increased number of vortex particles is approximated by pseudo-particles. However, the decrease in $\widetilde{W}$ leads to an increase in T_o as the computational effort related to the setup ($\approx 23\%$ of T_o) and the sweep ($\approx 76\%$ of T_o) of the octree rises. As a result, the wall time T is increased compared to the reference case, although $\widetilde{W} < \widetilde{W}_{ref}$. If the number of particles per box is increased to $n_{P,Box} = 20.000$ the work load ratio rises, too. In this case, the octree consists of larger boxes, only a few meet the distance criterion. Therefore, the number of P2P-interactions is higher than that of the reference case, which causes the wall time T to be larger than T_{ref}. Obviously, there is a trade-off between the reduction of the wall time T and the increase of wall time T_o linked to the VPPM's overhead. Therefore, the VPPM's break-even point strongly depends on the subdivision of the computational domain.

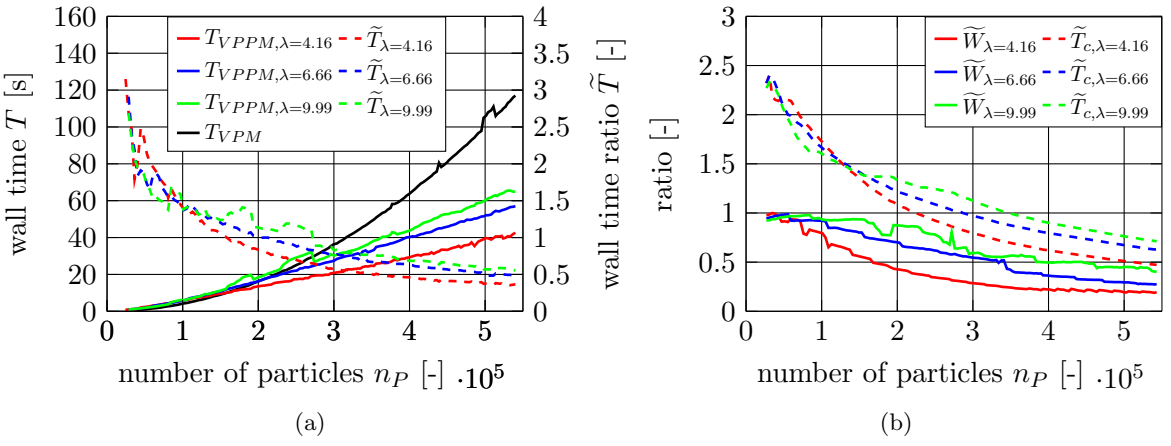

Figure 3: Comparison of wall time T and wall time ratio $\widetilde{T}$ for the P2P-calculation of the induced velocity (a) and cumulative wall time ratio T_c and work load ratio $\widetilde{W}$ (b) as a function of the number of particles for different tip-speed ratios

Besides the parameter $n_{P,Box}$, the VPPM's performance is also influenced by the length parameter l_{Top}. Since it defines the size of the boxes on the top level, it might be used similar to $n_{P,Box}$ to control the octree's refinement. However, its primary use is to take control of the

aspect ratio Λ of the cells on all levels. As described in Section 2.3, an enclosing sphere is defined for each box of the octree. Its radius r_{sphere} determines the minimal distance to the point of interest to be able to use a pseudo-particle representation of vortex particles, which are enclosed by the sphere. Therefore, to decrease $\widetilde{W}$, each box should feature two characteristics. First, it should cover a large volume to enclose a maximum number of particles, which will be represented by pseudo-particles. Second, it should have a small radius to be able to interact with a maximum of its surrounding particles. These contrary conditions are most efficiently met at the same time if the boxes are cube-shaped ($\Lambda = \Delta y/\Delta x = \Delta z/\Delta x = 1$). Figure 4b shows the influence of the aspect ratio on the wall time T and the work load ratio $\widetilde{W}$. The splitting of the boxes is disabled for the depicted cases except for the top level boxes, which are divided once. If the aspect ratio is $\Lambda = 1/3$, i.e., $\Delta y/\Delta x = \Delta z/\Delta x = 1/3$, the performance of the VPPM decreases since the fraction of the number of boxes that meet the distance criterion Eq. 10 is reduced. Thus, the aspect ratio of all boxes of the octree should be kept close to $\Lambda = 1$.

Although the length parameter l_{Top} was introduced to specify the boxes' aspect ratio, it interacts with the parameter $n_{P,Box}$. For the three cases of tip-speed ratios λ shown in Figure 3a, the savings in terms of computing time of the VPPM are best in case of $\lambda = 4.16$ although all simulations share the same setup (see Tab. 1). This is due the difference in the length of the rotor wake l_w for a fixed number of revolutions. Since $l_{w,\lambda=4.16} > l_{w,\lambda=6.66} > l_{w,\lambda=9.99}$ and the number of particles is nearly the same for all three cases, the number of particles per box on the top level is the lowest in the case of $\lambda = 4.16$. In contrast to the cases of $\lambda = 6.66$ and $\lambda = 9.99$, the threshold of $n_{P,Box} = 5000$ is never exceeded for $l_{Top} = 2.25m$ and there is no additional refinement of the octree's top level boxes. Therefore, the number of boxes is always lower in case of $\lambda = 4.16$ for the setup of the simulations used. At the same time, the distance criterion Eq. 10 is met for a larger fraction of the vortex particles, which yields a small $\widetilde{W}$. Consequently, the performance of the VPPM in case of $\lambda = 4.16$ is the best of all three cases for the used combination of $n_{P,Box}$ and l_{Top}.

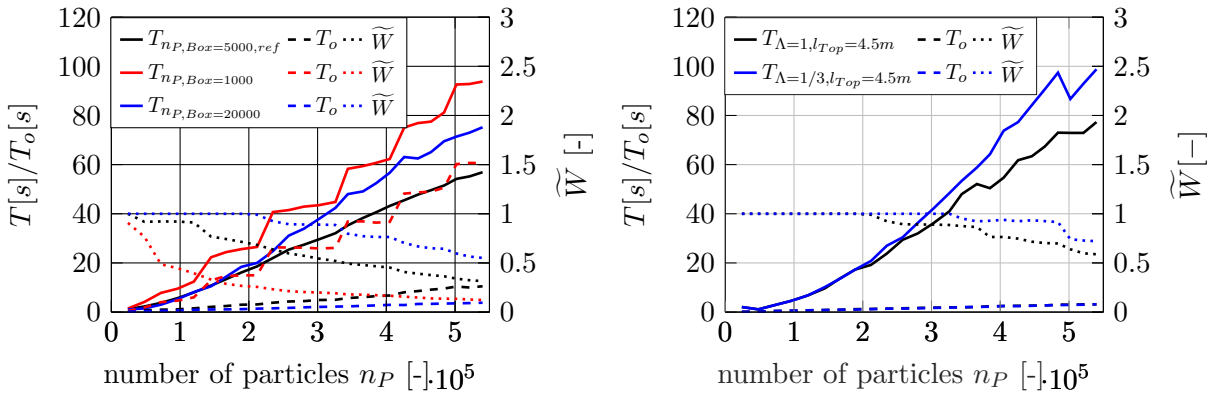

(a) (b)

Figure 4: Influence of the number of particles per box $n_{P,Box}$ (a) and the aspect ratio of the boxes (b) on the wall time T, the overhead's time T_o and the work load ratio $\widetilde{W}$

3.2. Error estimation

Since fractions of the P2P-interactions are represented by pseudo-particles using finite-series expansions, the VPPM's application induces an error compared to the VPM. The size of this truncation error depends on the cut-off order p, the sphere radius multiplier m_r, and the thresh-

old factor m_d defined in Section 2.3. To estimate the impact of these parameters, their influence on the error in the induced velocity is evaluated. For this purpose the particle field, which is obtained after 25 rotor revolutions using the VPM for $\lambda = 6.66$, is selected. The induced velocity is calculated at each particles' position by the VPM and VPPM. The error for different configurations of p, m_r, m_D is listed in Tab. 2. It turns out that a reduction of the cut-off order increases the error. The same applies to a decrease of m_r. This is because in both cases the approximation of physical particles through pseudo-particles deteriorates. If the threshold m_D is lowered, the error increases because the accuracy of the pseudo-particle approximation drops with decreasing distance to the point of interest. However, increasing the sphere radius multiplier or the threshold m_D decreases the performance of the VPPM since the fraction of particles, whose influence can be approximated during the calculation of the P2P interaction, is reduced. Therefore, there is a strong trade-off between the accuracy and the performance of the VPPM.

p	m_r	m_D	relative error [%]		absolute error [m/s]	
			mean	maximum	mean	maximum
7	1.5	1	0.37	26.76	0.02	0.05
5	1.5	1	0.38	29.20	0.02	0.05
7	1	1	0.68	47.40	0.04	0.09
7	2	1	0.23	14.96	0.01	0.03
7	1.5	0.5	0.61	32.03	0.04	0.08
7	1.5	1.5	0.25	17.37	0.01	0.03

Table 2: Magnitude of the error in the induced velocity for a variation of the parameters p, m_r, m_d

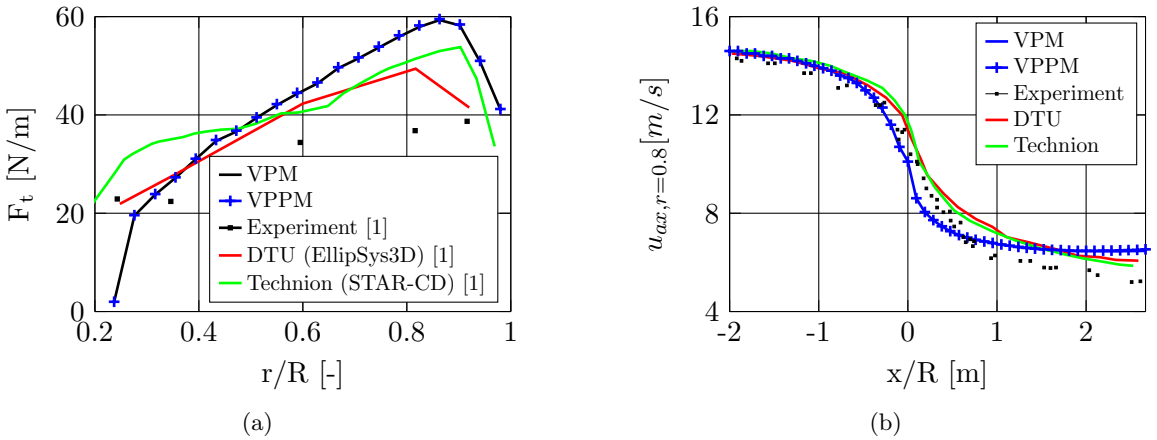

(a) (b)

Figure 5: Radial distribution of the rotor blade's tangential force calculated by the VPM and VPPM (a) and comparison of the axial velocity distribution inside the rotors wake after a simulation of 25 rotor revolutions ($\lambda = 6.66$) (b)

Obviously there is an error in the aerodynamic forces which is linked to the VPPM's truncation error. However, the comparison of the radial distribution of the rotor blade's tangential force after 25 rotor revolutions in Figure 5a shows that there is hardly any difference between the results of the VPPM and the VPM. The maximum error in the tangential force

distribution is 0.6%, while it is 0.3% for the normal force distribution. In addition, the axial velocity distribution in the rotor's wake, depicted in Figure 5b at a constant radius of r/R=0.8, shows that there is nearly no difference in the results of both methods, where the maximum error in the velocity u_{ax} is 1.2%. Consequently, the VPPM's induced error can be kept on a very low level.

4. Conclusions

To reduce the computational cost due to the n-body problem characteristic of vortex-particle methods an approach based on the Poisson Integral Method proposed by Anderson [8] has been presented. Finite-series expansions, which are represented by pseudo-particles and an octree structure are used in the calculation of the vortex particle-on-particle interaction (P2P). For the aerodynamic simulation of the MEXICO rotor [1] it is shown that the vortex pseudo-particle method (VPPM) is capable of significantly reducing the computational cost related to the calculation of the P2P-interaction ($\mathcal{O}(n_{Particles} \times log(n_{Particles}))$). Besides being advantageous in terms of reducing the computational cost the VPPM's implementation is quite simple compared to that of fast multipole methods since vortex and pseudo-particles share the same properties. Furthermore, no method specific boundary-conditions need to be imposed as in the case of multi-grid methods. Therefore, the presented vortex pseudo-particle approach is an attractive alternative to fast multipole or multi-grid methods.

5. Acknowledgements

The experimental data used have been supplied by the consortium which carried out the EU FP5 project MEXICO: 'Model rotor EXperiments In COntrolled conditions'. The consortium received additional support to perform the New Mexico measurements from the EU projects ESWIRP and INNWIND.EU.

References

[1] Schepers J, Boorsma K, Cho T, Gomez-Iradi S, Schaffarczyk P, Jeromin A, Shen W, Lutz T, Meister K, Stoevesandt B, Schreck S, Micallef D, Pereira R, Sant T, Aagaard Madsen H and Sørensen N 2012 *Analysis of Mexico wind tunnel measurements: Final report of IEA Task 29, Mexnext (Phase 1)* (Energy Research Centre of the Netherlands (ECN))
[2] Wellenberg W, Marnett M, Roidl B, Kirkendall D, Thönnißen F and Schröder W 2019 *Wind Engineering* **43** 639–656
[3] Greengard L and Rokhlin V 1987 *Journal of Computational Physics* **73** 325–348
[4] Berdowski T, Ferreira C and Walther J 2016 *Journal of Physics: Conference Series* **753** 032004
[5] van Garrel A 2016 *Multilevel panel method for wind turbine rotor flow simulations* Ph.D. thesis University of Twente
[6] Saverin J R, Marten D, Pechlivanoglou G and Paschereit C O 2018 *Journal of Physics: Conference Series* **1037** 062029
[7] Ramos-García N, Hejlesen M M, Sørensen J N and Walther J 2017 *Wind Energy* **20** 1871–1889
[8] Anderson C R 1992 *SIAM Journal on Scientific and Statistical Computing* **13** 923–947
[9] Makino J 1999 *Journal of Computational Physics* **151** 910–920
[10] Katz J and Plotkin A 2001 *Low-Speed Aerodynamics (Cambridge Aerospace Series)* (Cambridge University Press) ISBN 978-0-521-66219-2
[11] Winckelmans G and Leonard A 1993 *Journal of Computational Physics* **109** 247–273
[12] Cottet G H and Koumoutsakos P D 2000 *Vortex Methods* (Cambridge University Press)
[13] Winckelmans G S 2017 *Vortex Methods* (John Wiley & Sons)
[14] Pedrizzetti G 1992 *Fluid Dynamics Research* **10** 101–115
[15] Barnes J and Hut P 1986 *Nature* **324** 446–449